Structure of flame-made vanadia/titania and catalytic behavior in the partial oxidation of *o*-xylene

Bjoern Schimmoeller [a], Heiko Schulz [a,1], Anika Ritter [b,1], Andreas Reitzmann [b,2], Bettina Kraushaar-Czarnetzki [b], Alfons Baiker [c], Sotiris E. Pratsinis [a,*]

[a] *Particle Technology Laboratory, Department of Mechanical and Process Engineering, ETH Zurich, CH-8092 Zurich, Switzerland*
[b] *Institute of Chemical Process Engineering, Department of Chemical Engineering and Process Engineering, University of Karlsruhe (TH), D-76128 Karlsruhe, Germany*
[c] *Institute for Chemical and Bioengineering, Department of Chemistry and Applied Biosciences, ETH Zurich, CH-8092 Zurich, Switzerland*

Received 9 January 2008; revised 28 February 2008; accepted 1 March 2008

Available online 14 April 2008

Abstract

Vanadia/titania particles with a specific surface area (SSA) up to 195 $m^2 g^{-1}$ and a V_2O_5 content up to 40% (w/w) or V coverage up to 59 $V nm^{-2}$ were prepared by flame spray pyrolysis (FSP) under various conditions. The catalysts were characterized by nitrogen adsorption, X-ray diffraction, temperature-programmed reduction, and *in situ* Raman spectroscopy and tested for partial oxidation of *o*-xylene. Depending on vanadia content, monomeric, polymeric, and crystalline vanadia species were formed on TiO_2 support particles by FSP. Increasing the high-temperature particle residence time and concentration (production rate) during FSP reduced the SSA and increased the vanadia coverage of TiO_2 beyond a theoretical "monolayer" (>8–10 $V nm^{-2}$) while retaining amorphous (monomeric and polymeric) VO_x surface species. Controlling liquid precursor and dispersion gas feed rates, precursor concentration, and V_2O_5 content allowed the tailoring of SSA and the population of the different VO_x species in these vanadia/titania mixed oxides. For comparison, vanadia/titania catalysts containing 10% (w/w) V_2O_5 with comparable SSA and V coverage were prepared by impregnation, resulting in typical amorphous (<10 $V nm^{-2}$) and crystalline (>10 $V nm^{-2}$) VO_x species. Catalysts containing 7, 10, and 20% (w/w) V_2O_5 were deposited directly from the flame on ceramic foams that were tested for the partial oxidation of *o*-xylene to phthalic anhydride. The global activity of flame-made and conventionally impregnated catalysts depended mainly on SSA and vanadia loading (number of V surface sites), whereas the amorphous or crystalline nature of the VO_x species seemed to be less critical. In contrast, selectivity to phthalic anhydride was significantly affected by the nature of the VO_x species; amorphous species exhibited higher selectivity for conversion <90% compared with catalysts containing crystalline V_2O_5.
© 2008 Elsevier Inc. All rights reserved.

Keywords: Flame-spray pyrolysis; Flame-coated; Partial oxidation; Phthalic anhydride; Nanostructured V_2O_5/TiO_2; Ceramic foam; Ceramic sponge; *in situ* Raman spectroscopy

1. Introduction

Supported vanadia catalysts are used for various reactions, including selective catalytic reduction (SCR) of NO_x [1,2], oxidative destruction of volatile organic compounds (VOC) [1, 3], dehydrogenation of propane [4], and partial oxidation of *o*-xylene to phthalic anhydride (PA) [5], which is the focus of this study. Strong surface interactions between vanadia and titania result in amorphous monomeric, dimeric, and polymeric VO_x species that can be formed at sub-"monolayer" (<8–10 $V nm^{-2}$) coverage [6]. Exceeding that V coverage leads to crystalline V_2O_5 [5] regardless of preparation method, for example, classic impregnation [7], atomic layer deposition (ALD) [8], or even vapor-fed flame synthesis [9]. Crystalline V_2O_5 has a detrimental effect on activity and selectivity [10, 11]. Recently V_2O_5/TiO_2 catalysts prepared by flame-spray pyrolysis (FSP) showed good dispersion of vanadia while re-

taining the amorphous VO_x species up to a V coverage of 12 V nm^{-2} [12]. This catalyst with a specific surface area (SSA) of 53 m^2 g^{-1} showed higher selectivity at a given conversion than a sub-"monolayer" (7 V nm^{-2}) catalyst with higher SSA (93 m^2 g^{-1}) also prepared by FSP. These results encouraged us to systematically study the effect of V_2O_5 content, SSA, and nature of VO_x species in vanadia/titania catalysts for the partial oxidation of *o*-xylene.

The contributions of different VO_x species to the catalytic performance of vanadia-based catalysts has been debated for some time. At low loadings (up to 2–3 V nm^{-2}), strongly bound monomeric VO_x groups with three V–O bonds to the support and a terminal partly hydrated V=O bond are formed at ambient conditions [13]. At V coverage greater than about 3 V nm^{-2}, some V–O-support bridges rearrange themselves into V–O–V bridges [5,6,8] increasing the degree of polymerization. These still-amorphous vanadia species turn into crystalline ones when the V coverage exceeds about 8 V nm^{-2} [5]. Many researchers claim that amorphous monomeric VO_x species with terminal V=O bonds are the most active species for reactant adsorption and C–H bond breaking, particularly when compared with crystalline V_2O_5 [10,14–16]. In contrast, Gervasini et al. [8] found higher catalytic activity for polymeric rather than monomeric VO_x species in partial oxidation of *o*-xylene to PA. Weckhuysen and Keller [17] stated that the V–O-support bond is important in methanol oxidation, a model reaction for V_2O_5/TiO_2 catalysts. Recently, density functional theory (DFT) has demonstrated that the oxygen atom in the V–O–Ti bond is the most reactive toward H adsorption [18], the limiting step of the oxidation reaction, because of the high stability of terminal V=O bonds.

The influence of amorphous monomeric or polymeric and crystalline VO_x species on PA selectivity remains unclear. Pure crystalline V_2O_5 catalysts with high SSA (25 m^2 g^{-1}) exhibited higher selectivity and activity than corresponding catalysts with low SSA (1.8 m^2 g^{-1}) at constant residence times [19]. In contrast, Bond [14] reported that crystalline V_2O_5 does not affect catalytic activity and selectivity, and that the latter is influenced mainly by SSA. Evaluation of sub-monolayer (<8–10 V nm^{-2}) V_2O_5/TiO_2 catalysts prepared by ALD and classic impregnation showed that the higher selectivity during partial oxidation of *o*-xylene can be attributed to polymeric VO_x species rather than to monomeric species [8]. In industry, however, *o*-xylene catalysts have low SSA (7–30 m^2 g^{-1}) with high vanadia loadings of 5–15% (w/w), preferably around 7–10% (w/w) [14,20,21] exceeding the monolayer coverage often by a factor of >5 (V coverage >50 V nm^{-2}).

Here we prepared vanadia/titania catalysts with high V coverage and amorphous VO_x species by FSP and investigated the influence of such FSP variables as precursor concentration, liquid feed rate, and V_2O_5 content on the structural and catalytic properties of vanadia/titania mixed oxides. The catalytic materials were directly deposited onto ceramic foam carrier structures, and the effect of SSA and nature of VO_x species on activity and selectivity for the partial oxidation of *o*-xylene was investigated. Emphasis was placed on the elucidation of the crucial preparation variables determining the structural proper-

ties of the catalysts and on understanding how amorphous or crystalline VO_x species at high V coverage affect the catalytic performance. For comparison, catalysts with comparable SSA and V_2O_5 content were prepared by impregnation.

2. Experimental

2.1. Catalyst preparation

Nanostructured vanadia/titania particles were synthesized by FSP [22] of appropriate precursor solutions [12], resulting in titanium metal concentrations of 0.1–3.4 M and a nominal V_2O_5 content of 0–40% (w/w). Two FSP conditions were used, low enthalpy (LE: 5 mL min^{-1} liquid and 5 L min^{-1} O$_2$) and high enthalpy (HE: 8 mL min^{-1} liquid and 3 L min^{-1} O$_2$). FSP-made particles were directly deposited onto ceramic foam substrates for catalytic examination [12]. Particles that were not deposited onto the ceramic foam substrates were collected on glass microfiber filters (Whatman GF/D, 257 mm in diameter) by a vacuum pump (Busch SV 1025 B) for subsequent analysis. The pressure drop over foam and filter was adjusted to 80 mbar to achieve evenly distributed V_2O_5/TiO_2 coatings on the foam carrier [12]. The deposition time was in the range of 20–300 s.

For comparison, 10% (w/w) vanadia/titania reference catalysts were prepared by standard impregnation [23] of commercially available TiO$_2$ [TiO$_2$, >99.5% (w/w) anatase, Millennium PC50 (45 m^2 g^{-1}) and PC100 (82 m^2 g^{-1})]. Vanadia (Fluka, purity >99%) was dissolved in deionized water containing oxalic acid (Fluka, purity >99%, molar ratio V_2O_5:oxalic acid = 1:4), and an appropriate amount of titania was added to the solution. The suspension was mixed for several hours at 80 °C, after which water was evaporated. The material was dried at 65 °C in air overnight, crushed, fractionated (0.114 to 0.5 mm), and finally calcined in air (1 h, 450 °C, 1 °C min^{-1}).

2.2. Catalyst characterization

The SSA (m^2 g^{-1}) of the flame-made powders was determined by nitrogen adsorption (Pan Gas, >99.999%) using the BET method and a Micromeritics Tristar 3000 instrument. SSAs of the powders could be reproduced within 2.4%. X-ray diffraction (XRD) was performed on a Bruker D8 Advance diffractometer (step size of 0.03°, scan speed of 0.60° min^{-1}, Cu$K\alpha$ radiation). Weight content and crystal size of titania phases were obtained by Topas 2.0 software (Model AXS 2000, Bruker) as described in [12]. Temperature-programmed reduction (TPR) experiments were carried out on a Micromeritics Autochem II 2920 unit equipped with a thermal conductivity detector by flowing 5 vol% H$_2$ in Ar (Pan Gas, >99.999%, 20 mL min^{-1}) through the sample [12]. TEM analysis was performed with a CM30ST microscope (Philips; LaB$_6$ cathode, operated at 300 kV, point resolution ~2 Å) [12].

Raman spectroscopy was performed with a Renishaw InVia Reflex Raman system equipped with a 514-nm diode laser (Ar-ion laser; 25 mW) as the excitation source focused in a microscope (Leica, magnification ×5). The spectra were recorded under dehydrated conditions for 20–65 s and 10–25 accumulations

Table 1

Symbols, preparation conditions, BET, TPR results, k_m and $S_{PA,o}$ at $X_o = 0.6$ for all tested V_2O_5/TiO_2 catalysts from different preparation methods. Number in parenthesis indicate the initial SSA of the commercial TiO_2 support

Sample	Symbol (Figs. 7–10)	V_2O_5 content (% w/w)	Precursor TTIP concentration (mol L^{-1})	SSA ($m^2 g^{-1}$)	V-coverage (#nm^{-2})	dominant VO_x-species[a]	TPR T_{max} (°C)	AOS	k_m[b] ($cm^3 s^{-1} g_{cat}^{-1}$)	$S_{PA,o}$ at $X_o = 0.6$ (–)	Ref.
7V95-5	–	7	0.67	95	5	Amorphous	490	3.2	239.8	0.47	This work
10V93-7	▽	10	0.67	93	7	Amorphous	495	3.5	251.7	0.43	[12]
20V73-19	□	20	0.67	73	19	Amorphous/ crystalline	536	3.3	214.4	0.34	This work
10V53-12	⋈	10	3.4	53	12	Amorphous	520	3.6	120.4	0.47	[12]
10V40-16 HE-FSP	△	10	0.67	40	16	Amorphous	533	3.3	102.7	0.55	This work
10V24-27 HE-FSP	◇	10	3.4	24	27	Amorphous	497, 558	3.5	62.4	0.59	”
10V65-8 imp	◆	10	–	65 (82)[c]	8[d]	Amorphous	510	3.0	206.7	0.46	”
10V40-16 imp	▲	10	–	40 (45)[a]	16[d]	Crystalline	527	3.2	114.8	0.48	”
10V9-74 imp	●	10	–	9 (9)[c]	74[d]	Crystalline	546, 694	3.6	14.0	0.52	[12]

[a] Based on Raman analysis in Figs. 3, 4, and 5.
[b] Calculated for first-order reaction kinetics up to a $X_o = 0.6$ consistent with experimental data till this X_o.
[c] Initial SSA for the impregnated catalysts.
[d] Calculated for the initial SSA before impregnation.

to obtain sufficient signal-to-noise ratios, and collected on a CCD camera after being diffracted by a prism (1800 lines/mm) using 1.25 mW laser energy, to avoid thermal alteration [24, 25]. The procedure was as follows. First, samples were placed in a special *in situ* cell equipped with a quartz window. The samples were heated stepwise (50 °C steps, 10 °C min^{-1}) up to 350 °C while flushing with synthetic air (PanGas, 99.999%, 25 mL min^{-1}). Spectra were recorded at different temperatures (100, 200, 250, 300, and 350 °C) and after the cell was cooled. Spectra labeled "hydrated" were obtained before heating. The spectra did not change from 350 °C to ambient temperatures but showed better signal-to-noise ratios; therefore, all of the Raman spectra shown are reported after dehydration and cooling to 20 °C in the *in situ* cell unless stated otherwise.

Samples are labeled as xVy-z, where x, y, and z denote V_2O_5 content (% (w/w)), SSA ($m^2 g^{-1}$), and V atom coverage (#nm^{-2}), respectively (Table 1). One as-prepared catalyst (10V24-7) was subjected to an additional heat treatment between 350 and 600 °C for 5 h (5 °C min^{-1} heating rate) in air in an oven (Carbolite, CWF 1300).

2.3. Catalytic tests

Partial oxidation of *o*-xylene was performed in an isothermal plug-flow fixed-bed reactor [12]. All gases (N_2, >99.996%, and O_2, >99.95%, Air Liquide) and liquid *o*-xylene (>99.0%, Fluka) were fed by mass-flow controllers (Bronkhorst). Temperature and inlet pressure were kept constant at 367 °C and 1.3 bar, respectively. The molar fractions of *o*-xylene and oxygen in the reactor feed were 0.005 and 0.2, respectively. Total gas flows ranged from 120 to 600 mL min^{-1} at standard conditions. Modified residence times (τ_{mod}, g_{cat} s cm^{-3}) were defined as the mass of vanadia/titania in the reactor divided by the total gas flow rate under reaction conditions [12]. Analysis of all organic species was performed by online gas chromatography (GC; HP 6890, capillary column: HP-5, 50 m long, 0.32 mm in diameter and 0.25 μm film thickness), whereas CO and CO_2 was measured by nondispersive IR spectroscopy
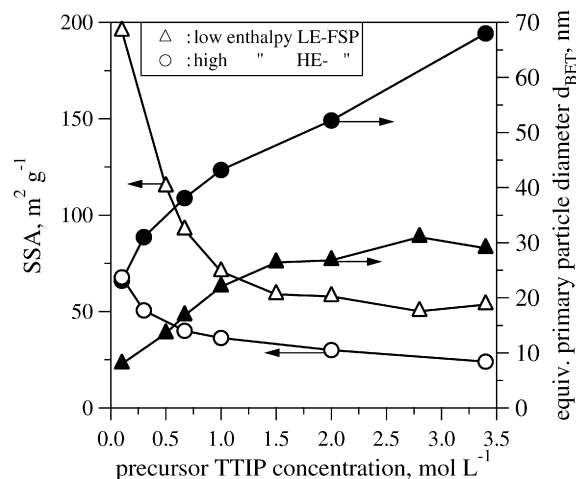

Fig. 1. Influence of TTIP precursor concentration (and flame enthalpy) in the FSP precursor liquid feed on the specific surface area (SSA, open symbols) and particle diameter (filled symbols) of 10% (w/w) V_2O_5/TiO_2 catalysts. Low enthalpy (LE) FSP corresponds to 5 mL min^{-1} precursor liquid and 5 L min^{-1} O_2 dispersion flow while high enthalpy (HE) corresponds to 8 mL min^{-1} liquid on 3 L min^{-1} O_2 flow.

(ABB; AO2020, Uras14). The carbon balance closed to ±5% and was additionally monitored by the CO_x content after catalytic combustion of organic species in a final total oxidation reactor [26]. Weisz numbers were found to be <0.6 for all catalysts, indicating that intraparticle mass transfer limitations can be excluded [12].

3. Results and discussion

3.1. Influence of preparation variables on structural properties of catalysts

Fig. 1 shows the influence of TTIP concentration in the FSP precursor solution on the SSA of 10% (w/w) V_2O_5-containing TiO_2 particles made by the LE (triangles) and HE (circles) FSP processes. The highest SSA (195 m^2 g^{-1}) was obtained
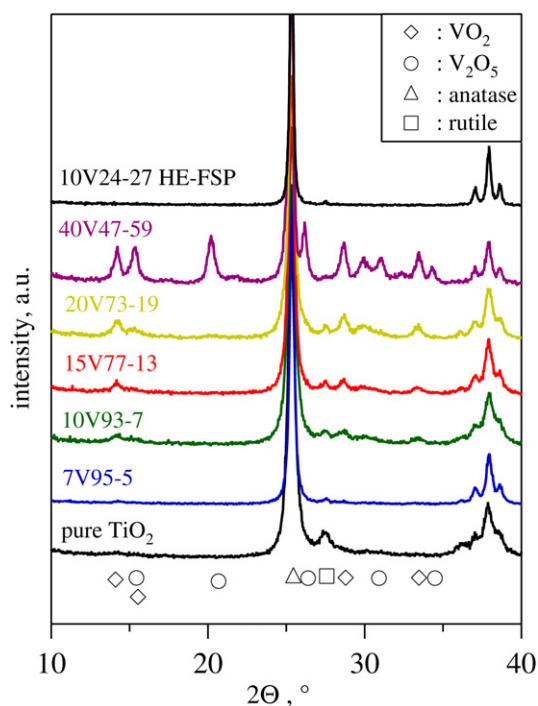
Fig. 2. XRD patterns (CuKα) of the 0–40% (w/w) V_2O_5 containing TiO_2 catalysts produced by low enthalpy FSP with 0 to high V-coverage (0–59 V nm^{-2}) as well as the XRD of the 10% (w/w) low SSA catalyst produced by high enthalpy FSP (HE-FSP).

using LE-FSP and a low Ti concentration (0.1 M, production rate 2.6 g h^{-1}). Increasing TTIP concentration up to 1 M resulted in a steep drop of SSA to 70 m^2 g^{-1}, which leveled off at around 53 m^2 g^{-1} ($d_{BET} \approx 28$ nm) at higher concentrations (2–3.4 M) [12]. This is attributed to faster particle growth at higher particle concentrations and to longer high-temperature particle residence time in the flame, favoring particle coagulation and coalescence, reducing the overall specific surface area in the flame, as has been reported for flame-made materials [22,27]. At about 2 M TTIP in the LE-FSP solution, primary particles of 28 nm average diameter were formed. Their characteristic sintering time might be too long [28] compared with their high-temperature residence time in the flame; thus, any further increase in TTIP and, subsequently, particle concentration did not increase the particle size, resulting in similar SSAs [29]. For HE-FSP, the SSA of the powder was reduced further compared with that in LE-FSP, in agreement with FSP-made CeO$_2$ [22]. Thus, controlling such production parameters as precursor concentration, liquid feed rate, and dispersion gas feed rate allowed us to tailor the characteristics of the catalysts [30]. The SSA decreased from 93 to 73 m^2 g^{-1} when the V_2O_5 content was increased from 1 to 20% (w/w) and dropped to 47 m^2 g^{-1} for a 40% (w/w) V_2O_5 content. As a previous study of flame-made V_2O_5/TiO$_2$ catalysts has shown [9], the vanadia forms a shell-like structure onto a TiO$_2$ core rather than a solid solution of V atoms in the TiO$_2$ matrix in a flame, thereby increasing the VO$_x$ surface population density with decreasing SSA.

Fig. 2 shows XRD patterns of the 1–40% (w/w) V_2O_5-containing TiO$_2$ particles produced by LE-FSP and a 24 m^2 g^{-1} 10% (w/w) V_2O_5-containing TiO$_2$ catalyst made by HE-FSP.

Line broadening of the XRD patterns indicates anatase crystals of 17–37 nm, in close agreement with the calculated BET diameter (Fig. 1), hinting at the presence of monocrystalline grains or primary TiO$_2$ particles. At 7% (w/w) vanadia content, weak reflections corresponding to crystalline VO$_2$(B) (diamonds) appeared. Quantification of this phase was not possible, because pure TiO$_2$ exhibited small and broad diffractions at these angles (14.2°, 28.4°, 33.4°) which can be attributed to a high-pressure phase TiO$_2$(B) with a similar lattice structure and cell size [31]. Nevertheless, the increase in peak intensities at these angles with increasing V_2O_5 content may indicate the presence of a small fraction of crystalline VO$_2$(B), at least for V_2O_5 content >7% (w/w) for the LE-FSP-made catalysts.

The patterns of as-prepared 20% (w/w) V_2O_5/TiO$_2$ catalyst showed high anatase content with no crystalline V_2O_5 structure despite the relatively high V coverage (19 V nm^{-2}); in contrast, at a 40% (w/w) V_2O_5 content, crystalline V_2O_5 was detected (circles). TEM and EELS analysis (not shown) indicated separate V_2O_5 particles, suggesting that at higher V contents, at least a fraction of the vanadia nucleates homogeneously as individual particles, in addition to those condensing heterogeneously on the earlier-formed TiO$_2$ [9]. Despite the high V coverages of 16 and 27 V nm^{-2}, XRD patterns of the HE-FSP catalysts showed no diffraction lines attributed to crystalline VO$_2$ or V_2O_5 (Fig. 2 top), whereas a high anatase fraction [>98% (w/w)] was observed with crystallite sizes comparable to the BET diameter, indicating monocrystalline particles as well. The XRD patterns (not shown) of impregnated catalysts [10% (w/w) V_2O_5 content] showed no diffraction lines due to crystalline vanadia for both high-SSA samples (65 m^2 g^{-1}, 8 V nm^{-2}) and low-SSA samples (40 m^2 g^{-1}, 16 V nm^{-2}), and the initial anatase weight fraction was preserved.

Fig. 3 shows Raman spectra of dehydrated V_2O_5/TiO$_2$ catalysts made by LE-FSP. The two overtone bands (514 and 638 cm^{-1}) corresponding to anatase TiO$_2$ were clearly visible for all of the flame-made catalysts. The band at around 800 cm^{-1} stems from the Si–O–Si vibration of the quartz window used in the *in situ* cell. At very low V coverage (1 V nm^{-2}, 1V93-1), a V=O stretching band at 1032 cm^{-1} attributed to monomeric VO$_x$ [13] was detected. With increasing V coverage up to 15% (w/w) V_2O_5, a band at around 920–940 cm^{-1} appeared that can be attributed to the V O–V bridges of the polymeric VO$_x$ species [6,17,32–35]. These bands (at 1032 and 940 cm^{-1}) allow no conclusion on the ratio between monomeric and polymeric species, because they hardly change in intensity with increasing V_2O_5 content. The characteristic behavior of first monomeric, then polymeric (decreasing monomeric) VO$_x$ species, and finally crystalline V_2O_5 forming with increasing V coverage also seems to hold for flame-made V_2O_5/TiO$_2$ catalysts. The 1V93-1 sample showed no indication of monomeric, but clear bands of polymeric (940 cm^{-1}) VO$_x$ species under ambient (hydrated) conditions (not shown here).

At higher V content (i.e., sample 15V77-13), Raman bands of amorphous monomeric and polymeric VO$_x$ species remained dominant. For the 20V73-19 catalyst, features of amorphous VO$_x$ species were still detected, along with additional Raman shifts (at 708 and 998 cm^{-1}) attributed to crystalline V_2O_5 that
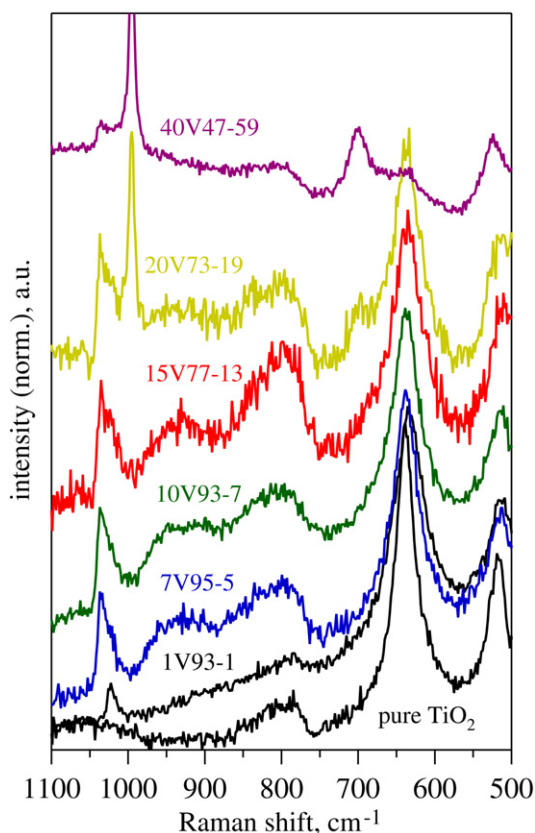
Fig. 3. Raman spectra of the FSP-made 0–40% (w/w) V_2O_5 containing TiO_2 catalysts made by LE-FSP recorded (514 nm) after dehydrating the sample at 350° (by flowing 25 mL min^{-1} synthetic air).
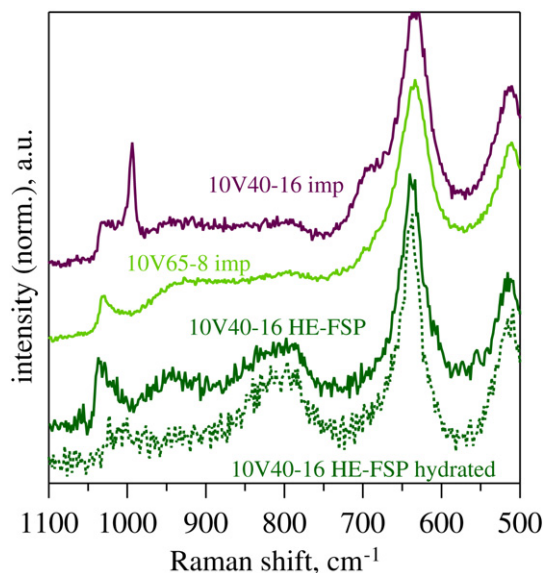

Fig. 4. Raman spectra of the 10% (w/w) V_2O_5 HE-FSP and impregnated catalysts recorded (514 nm) after dehydrating the sample at 350° (by flowing 25 mL min^{-1} synthetic air). The spectra of the 10V40-16 HE-FSP are shown also under ambient (hydrated) conditions (dotted line).

were not detected by XRD (Fig. 2). This finding corroborates the relative small size of crystalline V_2O_5 clusters in flame-made catalysts even at relative high V coverage. Doubling the V_2O_5 content [40% (w/w)] resulted in dominantly crystalline Raman bands, consistent with XRD (Fig. 2) and TEM/EELS analysis (not shown). The dominant Raman shifts and scattering arising from the TiO_2 support and additional overlap with V_2O_5 bands prevented detection of discrete major VO_2 bands expected at 191, 258, and 335 cm^{-1} [36] and thus could not clarify the origin of the XRD patterns attributed to either $VO_2(B)$ or $TiO_2(B)$, respectively.

Fig. 4 shows Raman spectra (solid line) of both dehydrated HE-FSP-made 10V40-16 and impregnated (10V65-9 imp, 10V40-16 imp) V_2O_5/TiO_2. The flame-made catalyst exhibited a clear band at 1033 cm^{-1} that corresponds to monomeric VO_x species [13]. as well as a band at 940 cm^{-1} confirming the presence of amorphous polymeric VO_x species [32] stemming from the higher V coverage (16 V nm^{-2}) of HE-FSP-made particles. Missing bands at 703 and 998 cm^{-1} indicated the absence of any crystalline V_2O_5 species despite the relatively high V coverage. This is in contrast to the classic "monolayer" model for impregnated catalysts [5] and vapor-fed flame-made 10% (w/w) V_2O_5/TiO_2 with slower gas velocities and longer high-temperature particle residence times [9]. Note the missing band at 940 cm^{-1} for the hydrated sample (dotted line) and higher intensity around 800 cm^{-1}, which may indicate the addition of

polymeric VO_x species as was observed under ambient conditions (not shown) to the signal arising from the quartz window, as discussed in Fig. 3.

Raman spectra of the impregnated high-SSA V_2O_5/TiO_2 (10V65-8 imp) showed weaker intensities for the monomeric and polymeric VO_x species (Fig. 4) compared with the FSP-made catalysts. For the impregnated low-SSA catalyst (10V40-16 imp), only monomeric and almost no intensities of bands indicative of polymeric VO_x species were detected; instead, crystalline V_2O_5 Raman bands at 703 and 998 cm^{-1} were observed, in contrast with the HE-FSP-made catalyst with comparable SSA and V coverage (10V40-16 HE-FSP). Crystalline V_2O_5 particles were again too small to be detected by XRD, but their presence is consistent with impregnated catalysts with >8 or 10 V nm^{-2} [5,25].

Fig. 5 shows Raman spectra of the catalyst with the lowest SSA and highest V atom coverage (10V24-27 HE-FSP). The dehydrated sample showed similar monomeric and polymeric bands as the HE-FSP-made 40 m^2 g^{-1} catalyst (Fig. 4). Again, no bands corresponding to crystalline V_2O_5 could be detected despite the relative high V coverage of 27 V nm^{-2}. Apparently high cooling rates (up to 10^6 °C s^{-1} [37]) and short high-temperature residence times favored the formation of a thin layer of amorphous VO_x over crystalline V_2O_5. In addition, V_2O_5 is very volatile ($T_{melt} \approx 670$ °C) compared with TiO_2 ($T_{melt} \approx 1800$ °C), so it should condense on the TiO_2 surface late in the flame [9], reducing the high-temperature residence time of the mixed V_2O_5/TiO_2 particles and thereby preventing the development of crystalline layers

Fig. 6 shows typical TEM images of these particles. Pure TiO_2 produced at 5 mL min^{-1} (LE-FSP) and a precursor concentration of 0.67 M (Fig. 6a) showed predominantly spherical particles with a low degree of aggregation. Adding 20% (w/w) V_2O_5 had no effect on the particle shape and aggregation

state even though particle size increased by 25%. Even the HE-FSP-made 10V24-27 catalyst exhibited no significant structural changes, except for the larger particle size. This indicates that the structure of TiO_2 particles was not affected by adding V_2O_5, and that the formation of the TiO_2 was completed before the condensation of V_2O_5 on the particle surface, in agreement with other flame-made V_2O_5/TiO_2 catalysts [9,12].

Because the 10V24-27 HE-FSP-made catalyst exhibited the highest theoretical "monolayer" coverage of the tested catalysts, it was most sensitive to any heat treatment, such as during reaction or after treatment (e.g., calcination). To characterize the stability of the detected amorphous VO_x species in the as-prepared sample, the sample was annealed in air at different temperatures (Fig. 5). At 450 °C (significantly higher than the *o*-xylene reaction temperature of ca. 370 °C and similar to the calcination temperature of impregnated catalysts) no changes in the bands attributed to amorphous VO_x species at 940 and 1032 cm^{-1} were observed, corroborating the stability of such species in FSP-made catalysts. Bands corresponding to crys-
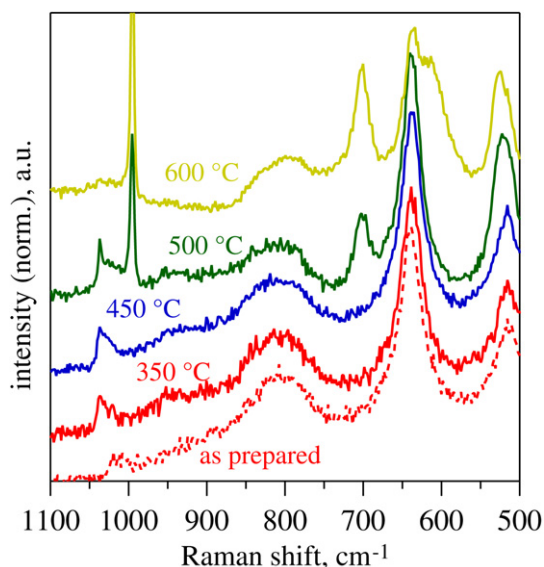
talline V_2O_5 were detected after annealing at 500 °C, in agreement with previous results for a sintered FSP-made high-SSA (10V93-7) catalyst [12]. All bands (monomeric, dimeric, and polymeric) attributed to amorphous VO_x species were still visible, in contrast to the 10V93-7 catalyst.

At 600 °C, the bands due to monomeric species disappeared, but amorphous polymeric VO_x species were retained, and the crystalline bands became more distinct. In addition, the anatase (638 cm^{-1})-to-rutile (608 cm^{-1}) phase transformation began, in agreement with the XRD results. This is in contrast to the 10V93-7 catalyst with higher SSA, in which this transformation had been completed at this temperature [12]. At the same time, the SSA of the catalyst was reduced from 22 to 7 m^2 g^{-1}. These findings indicate that low-SSA catalysts made by HE-FSP are more stable in terms of VO_x species, particle size, and anatase to rutile transformation on heat treatment compared with high-SSA catalysts made by LE-FSP, because the larger initial TiO_2 particle sizes lead to slower sintering and phase transformation [28,38].

Fig. 7a shows the TCD signals measured during TPR of the 0–100% (w/w) V_2O_5-containing TiO_2 catalysts. At low V coverage (1 V atom nm^{-2}), the maximum reduction peak temperature (T_{max}) was around 500 °C. Increasing the V_2O_5 content from 1 to 7% (w/w) reduced the T_{max} to 490 °C (5 V nm^{-2}), indicating greater overall reducibility of the VO_x species present at this V coverage. This corroborates the Raman results under ambient conditions, which demonstrated polymeric VO_x species at low coverage (1 V atom nm^{-2}) and easily reducible monomeric species at a content of 5–15% (w/w). Further increases in the V_2O_5 content increased T_{max} up to 595 °C for the 40% (w/w) with 59 V nm^{-2}, indicating lower reducibility of the high-coverage VO_x species. But part of this shift in the peak temperature must be attributed to the increasing amount of reducible species, as parametric sensitivity TPR studies have indicated [39]. All catalysts up to 20% (w/w) V_2O_5 showed only slightly asymmetric reduction peaks, whereas the 40% (w/w) V_2O_5 sample showed a clear shoulder around 565 °C, indicating a stepwise reduction or differing reducibilities of the corresponding VO_x species. TPR of the pure FSP-made V_2O_5 showed the two characteristic reduction peaks of crystalline vanadia at around 650–750 °C.

Fig. 5. Raman spectra of low SSA, high "monolayer" coverage 10V24-27 V_2O_5-containing TiO_2 HE-FSP-made catalyst sintered at 350–600 °C for 5 h in air, recorded (514 nm) before (dotted line) and after dehydrating the sample at 350° (by flowing 25 mL min^{-1} synthetic air).
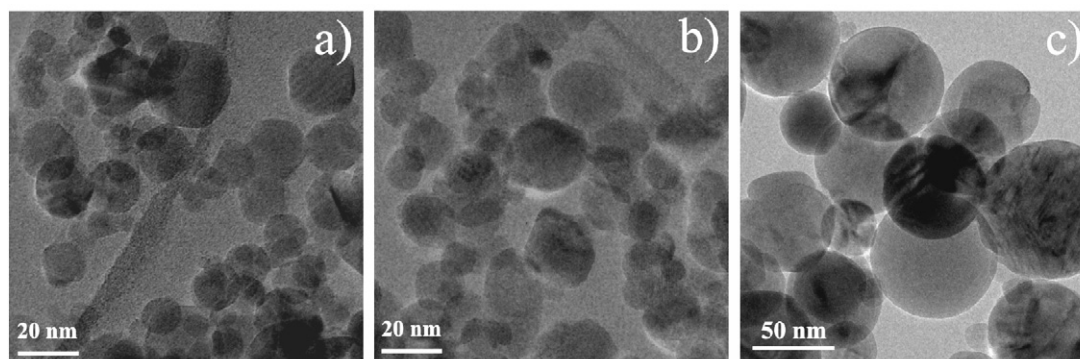

Fig. 6. TEM images of (a) pure FSP-made TiO_2 (98 m^2 g^{-1}, 0.67 M TTIP, LE-FSP), (b) 20% (w/w) V_2O_5/TiO_2 (20V73-19, 0.67 M TTIP, LE-FSP) and (c) 10% (w/w) V_2O_5/TiO_2 (10V24-27 HE-FSP, 3.4 M TTIP) catalysts.
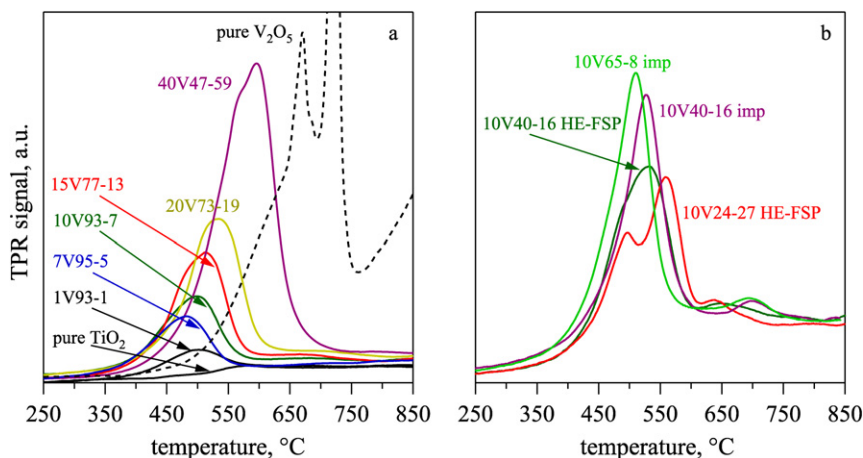
Fig. 7. (a) Temperature-programmed reduction (TPR) profiles of the FSP-made V_2O_5/TiO_2 catalysts shown in Fig. 2 as well as pure V_2O_5 made by LE-FSP. (b) TPR profiles of 10% (w/w) V_2O_5 containing FSP and impregnated catalysts of similar SSA.

Fig. 7b compares TPR results from as-prepared 10% (w/w) V_2O_5 containing TiO_2 HE-FSP-made and impregnated low-SSA catalysts. With increasing V coverage, the maximum reduction temperature for the 10V40-16 catalyst was shifted to 533 °C, with a shoulder around 495 °C stemming from the higher amount of polymeric VO_x species. For lower SSA (24 $m^2 g^{-1}$) and high V coverage (10V24-27), a split of the reduction profile into two distinct peaks at T_{max} = 497 and 558 °C was observed, further indicating reduction of different VO_x species, consistent with the Raman analysis of Fig. 4. The impregnated 10V40-16 catalysts containing crystalline vanadia (Fig. 4) showed similar reduction temperatures as the FSP-made catalysts of comparable SSA and V_2O_5 content that contained only amorphous VO_x species. This demonstrates that the reduction temperature was not significantly affected by the nature of VO_x species at this V coverage and small V_2O_5 cluster sizes. During reduction, the consumed H_2 was comparable for all FSP-made samples, and the calculated average oxidation state (AOS) was in the range of 3.2–3.5 for all catalysts (Table 1). The H_2 consumption of impregnated catalysts was slightly higher, and the resulting AOS ($\approx$3.0) was accordingly lower compared with FSP-made samples (Table 1).

3.2. Catalytic performance

Table 1 summarizes the characteristics of all catalysts investigated in this work, together with some samples reported earlier [12] for reference. This selection demonstrates the influence of vanadia content, type of VO_x species, SSA, and preparation route on the catalytic performance in the selective oxidation of o-xylene to phthalic anhydride. All catalysts showed no external or internal mass transfer limitations due to the relatively high gas velocity and the high porosity of the deposited active layer on the ceramic foam carriers [12]. Fig. 8 shows the o-xylene conversion, X_o, as a function of modified residence time of LE-FSP-made V_2O_5/TiO_2 deposited directly on foams and containing 7 and 20% (w/w) V_2O_5. Whereas the 7V95-5 (circles) showed comparable X_o at given residence times as the
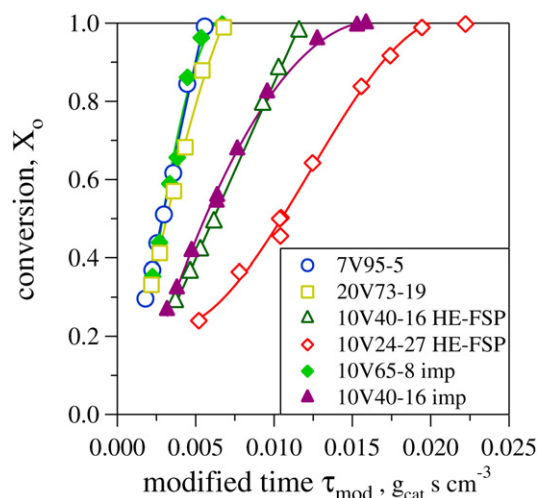

Fig. 8. Conversion of o-xylene as a function of the modified residence time at a reaction temperature of 367 °C for all tested catalysts (molar fraction of o-xylene = 0.005).

10% (w/w)-containing catalyst (10V93-7, Table 1) used in the previous study [12], slightly lower values were found for the 20V73-19 catalyst (cubes). This may be due either to the lower SSA or to the presence of crystalline V_2O_5 in the 20V73-19 catalyst (Fig. 3), which decreased its activity.

The 10V65-8 imp (filled diamonds) and 10V24-27 HE-FSP (open diamonds) catalysts exhibited the highest and lowest conversions, respectively, of the 10% (w/w)-containing V_2O_5 catalysts tested in the present study. Flame-made and impregnated 10V40-16 catalysts (triangles) of similar SSA showed intermediate conversions. Even though these two catalysts were prepared by different methods, contained different VO_x species (Fig. 4), and exhibited slightly different AOS (Table 1), they exhibited the same X_o. Similar conclusions can be drawn for the 20V73-19 LE-FSP and 10V65-8 imp catalysts despite the difference in VO_x species population (Figs. 3 and 4). This indicates that the nature of the VO_x species did not determine the X_o provided that the surface V coverage was at least 8 V atoms per nm^2.
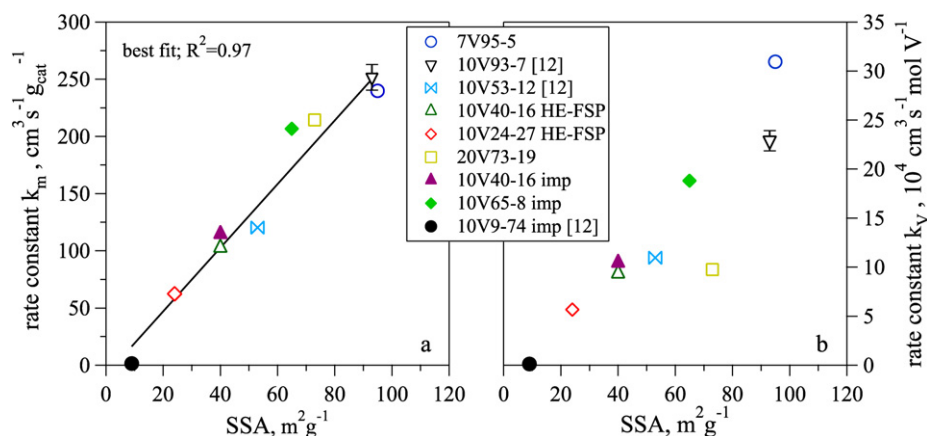
Fig. 9. Comparison of the calculated rate constants (first-order) for *o*-xylene conversion based on the catalyst mass (a, k_m) and on the amount of active species (b, k_V, mol V) for the catalysts prepared with different production rates and preparation methods in dependency of the SSA.

Fig. 9 shows a clear relationship between catalyst activity and SSA. First-order reaction kinetics for the calculation of the rate constant k_i were assumed, even though the partial oxidation of *o*-xylene does not strictly follow first-order kinetics [40,41]. But if we consider only the conversion up to $X_o = 0.6$, then the data can be seen to fit the first-order reaction kinetics in the $\ln(1 - X_o)$ versus τ_{mod} diagram reasonably well ($R^2 = 0.9$) and give a good estimate of the reaction rate constant. The calculated rate constant is shown as a function of SSA for the catalysts used here and in [12] (Table 1). In Fig. 9a, k_m is related to the mass of catalyst (V_2O_5/TiO_2) in the reactor and shows that the catalyst activity is well correlated ($R^2 = 0.97$) with its SSA, as also was observed for pure V_2O_5 [19]. Therefore, with increasing SSA, the activity increased linearly regardless of catalyst synthesis route, V_2O_5 content (V coverage), or VO_x species. Because both k_m and SSA are scaled by the mass, and because the number of V surface sites is proportional to SSA, our findings support the conclusion that only surface species, regardless of their type (monomeric or polymeric, amorphous or crystalline), are responsible for the activity of such V_2O_5/TiO_2 catalysts. In addition, the k_m dependency on the SSA may support the contention of Weckhuysen and Keller [17] and Calatayud and Minot [18] that the oxygen in the V–O–Ti bond is the most active in V_2O_5/TiO_2 catalysts. With decreasing SSA, less V–O-support groups are available. At increasing V coverage, such bonds become covered and may not be accessible for reaction.

In contrast, when the rate constant is related to the molar amount of V (k_V, Fig. 9b) nominally present in the catalysts and assumed to be the only active species, the differences between catalysts with differing vanadia content become apparent. This stands in contrast to the earlier statement that only surface VO_x species are important. The catalyst with the lowest coverage (7V95-5 LE-FSP, open circles, Fig. 9b) showed the highest activity. A further increase in V coverage while retaining high SSA (10V93-7 LE-FSP, inverted triangle) led to a reduction in catalyst activity. The V-based activity was reduced even more (∼30 %) for the 20% (w/w) V_2O_5-containing catalyst (19 V nm^{-2}, squares). But for all of the catalysts with 10% (w/w) vanadia, the k_V correlated very well with SSA ir-

respective of the preparation method used or the type of VO_x species present. Keeping in mind that the highest activity was observed at low V coverage regardless of rate-constant scaling, it is evident that the active VO_x species for the partial oxidation of *o*-xylene could form already at V coverage as low as 5 V atoms per nm^2. At comparable SSA, a further increase in V coverage had no effect on catalyst activity. This is in agreement with both the aforementioned hypothesis of Weckhuysen and Calatayud and the accepted "theory of towers" of Bond and Tahir [42], which posits that the V_2O_5 layer grows in tower-like structures on TiO_2. A correlation of the activity of V_2O_5/TiO_2 catalysts with V content is not conclusive, because the role of the bridging O-atoms is not taken into account. The activity depends predominantly on the SSA.

Fig. 10 shows that the selectivity to phthalic anhydride ($S_{PA,o}$) increased for all of the catalysts with increasing *o*-xylene conversion [12]. The PA is formed mainly as a consecutive product through the main intermediates tolualdehyde and phthalide (inset Fig. 10). The maximum $S_{PA,o}$ was observed at >90–95% conversion (X_o), indicating the high stability of PA against its consecutive oxidation to CO_x, as has been observed with V_2O_5/TiO_2 prepared by conventional methods [43]. Fig. 10a shows that increasing the V content of low enthalpy (LE) FSP-made catalysts lowered the $S_{PA,o}$ for X_o to <0.95. The $S_{PA,o}$ was higher for 7V95-5 (circles) than for 20V73-19 (squares) and for 10V93-7 (triangle), even though in the latter case both catalysts had almost the same SSA. This demonstrates that, in contrast to activity (Figs. 8 and 9), selectivity is affected by the type or content of vanadia. This conclusion is further supported by Fig. 10b showing catalysts with the same vanadia content [10% (w/w)] but prepared by different methods: The flame-made catalysts (10V40-16 and 10V24-27) were more selective than those prepared by impregnation (10V65-8 imp and 10V40-16 imp) at $X_o < 0.9$. For the impregnated catalysts, SSA had no significant effect on $S_{PA,o}$. In contrast, all of the flame-made catalysts containing 10% (w/w) vanadia, including 10V93-7LEF (Fig. 10a), showed decreasing $S_{PA,o}$ (up to X_o of at least 70%) with increasing SSA. Finally, 10V40-16 imp and 10V40-16 HEF exhibited the same SSA, but the latter flame-made catalyst (which contained amorphous
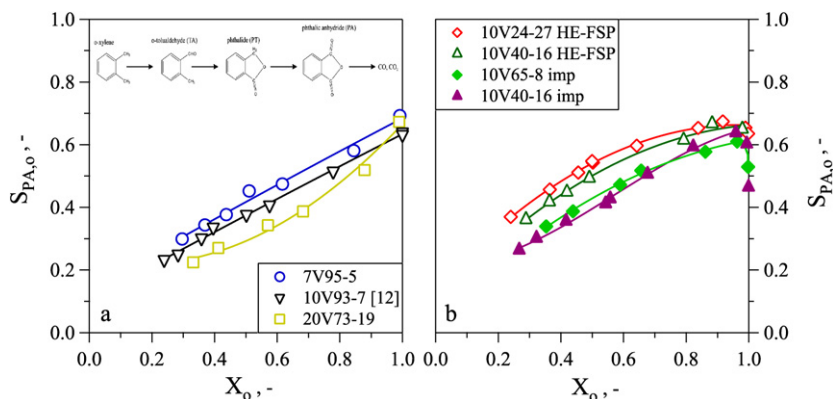
Fig. 10. Phthalic anhydride (PA) selectivity, $S_{PA,o}$ as a function of o-xylene conversion, X_o for 7, 10 and 20% (w/w) V_2O_5 containing (a) low enthalpy FSP-made catalysts. Inset shows simplified reaction diagram. (b) High enthalpy (HE) FSP (open symbols) and impregnated (filled symbols) catalysts at 367 °C reaction temperature and 0.005 molar fraction o-xylene in the feed.
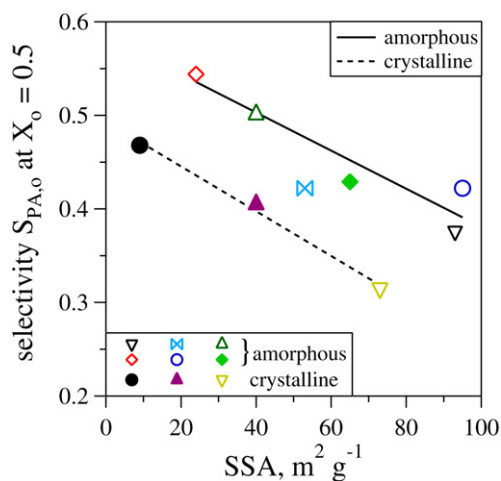

Fig. 11. Comparison of the PA selectivity at $X_o = 0.5$ for the tested catalysts prepared with different preparation methods as function of the SSA. Same symbols as in Fig. 9.

vanadia only; Fig. 4) yielded significantly higher $S_{PA,o}$ than the former impregnated catalyst.

Fig. 11 shows the effect of the type of VO_x species on PA selectivity in more detail. Here, $S_{PA,o}$ at 50% o-xylene conversion are plotted versus SSA, and two trend lines combine the data of catalyst samples with or without crystalline V_2O_5, respectively, as detected by XRD (Fig. 2) and Raman spectroscopy (Figs. 3, 4, and 5). At comparable SSA (and, accordingly, comparable catalytic activity), the presence of crystalline V_2O_5 had a detrimental effect on the $S_{PA,o}$ at intermediate X_o [14], consistent with the $S_{PA,o}$ at $X_o = 0.6$ reported in Table 1. This suggests that among the numerous species present on the TiO_2 surface, amorphous monomeric and polymeric species play the key roles in obtaining high PA selectivity. Nevertheless, catalysts are more selective at decreased SSA regardless of the VO_x species present [12]. Both of these findings are supported by the selectivities to side products obtained over all of the materials tested.

Higher SSA and crystalline V_2O_5 promoted the formation of o-tolualdehyde and phthalide (not shown). The CO_x selectivity

was almost constant (around 30%) over the entire X_o range for all tested catalysts except the 10V24-27 HE-FSP catalyst (for which this value was 20–25%). Although at $X_o = 90$–95%, the $S_{PA,o}$ became very similar in all of the catalysts (so that the dependency between catalyst properties and $S_{PA,o}$ could no longer be clearly discerned), the most selective catalysts at almost full o-xylene conversion exhibited high to moderate activity (SSA) and contained no crystalline V_2O_5, with the exception of 20V73-19 LE-FSP. The reason for the positioning of the 10V53-12 (butterfly) a bit away from the amorphous trendline is not entirely clear, but may be attributed to its slightly higher VO_2 content, as indicated by this sample's highest oxidation state of all the samples tested (Table 1).

Our findings in the present study demonstrate that FSP facilitates the preparation of mixed vanadia/titania catalysts with maximum content of dispersed amorphous VO_x and helps prevent the formation of crystalline V_2O_5, especially in catalysts with moderate SSA and V coverage (>8–10 V nm^{-2}). The FSP-made catalysts 10V40-16 and 10V24-27 with high V coverage (16 and 27 V nm^{-2}, respectively) demonstrated the highest PA selectivity ($S_{PA,o} = 67$–69%). This superior performance was observed both at intermediate conversion levels and at o-xylene conversions >90%.

4. Conclusion

In the present study, vanadia/titania nanostructured particles of various SSA (24–195 m^2 g^{-1}) and V coverage (5–59 V nm^{-2}) containing predominantly amorphous VO_x species <30 V nm^{-2} were prepared by FSP. The influence of preparation method (flame or impregnation), SSA, V content, and nature of the VO_x species (monomeric, polymeric, and crystalline) on the partial oxidation of o-xylene to phthalic anhydride (PA) was investigated. The major difference between flame-made and impregnated V_2O_5/TiO_2 particles lies in the state of the VO_x. As impregnated catalysts are calcined for long periods to ensure stability, the VO_x has sufficient time to form a thermodynamically stable crystalline phase. In corresponding FSP-made catalysts, the high-temperature residence time is too short to allow the development of crystalline V_2O_5,

especially at low [1–15% (w/w)] V content, and thus amorphous VO_x species are formed. These species remain stable even after similar heat treatment as for the impregnated catalysts during calcination. The fact that FSP reactors can operate at much higher maximum temperatures and cooling rates [37] compared with conventional vapor-fed reactors [9] may be why V_2O_5/TiO_2 particles made in the latter reactors formed crystalline V_2O_5 in this and previous studies [12].

The catalyst activity was found to strongly depend on SSA and thus also on the amount of surface V sites regardless of preparation method, V coverage, and nature of the VO_x species. Impregnated V_2O_5/TiO_2-containing crystalline V_2O_5 catalysts showed inferior selectivity for PA ($S_{PA,o}$) compared with FSP-made ones of similar composition and SSA. In general, higher activity was accompanied by lower $S_{PA,o}$ for o-xylene conversion (X_o) < 90%. High V_2O_5 contents (20% w/w) and SSA exhibited significantly lower $S_{PA,o}$ at X_o < 95%, whereas comparable $S_{PA,o}$ was obtained near full conversion. The $S_{PA,o}$ at $X_o = 50\%$ decreased linearly with increasing SSA for both amorphous and crystalline VO_x species; however, the catalysts containing amorphous VO_x species showed significantly higher selectivity compared with those catalysts with crystalline vanadia. The most selective catalysts for X_o < 90% had intermediate to low SSA and a high fraction of amorphous VO_x species. FSP has been shown to be a versatile method for the preparation of catalysts with a wide SSA range and controllable nature of VO_x species, which may not be achievable by classical wet-chemistry routes [30].

Acknowledgments

References

[1] G. Busca, L. Lietti, G. Ramis, F. Berti, Appl. Catal. B 18 (1998) 1.
[2] N.Y. Topsoe, H. Topsoe, J.A. Dumesic, J. Catal. 151 (1995) 226.
[3] G. Busca, M. Baldi, C. Pistarino, J.M.G. Amores, V.S. Escribano, E. Finocchio, G. Romezzano, F. Bregani, G.P. Toledo, Catal. Today 53 (1999) 525.
[4] A. Khodakov, B. Olthof, A.T. Bell, E. Iglesia, J. Catal. 181 (1999) 205.
[5] B. Grzybowska-Swierkosz, Appl. Catal. A Gen. 157 (1997) 263.
[6] G. Deo, I.E. Wachs, J. Haber, Crit. Rev. Surf. Chem. 4 (1994) 141.
[7] C.R. Dias, M.F. Portela, Catal. Rev. Sci. Eng. 39 (1997) 169.
[8] A. Gervasini, P. Carniti, J. Keranen, L. Niinisto, A. Auroux, Catal. Today 96 (2004) 187.
[9] W.J. Stark, K. Wegner, S.E. Pratsinis, A. Baiker, J. Catal. 197 (2001) 182.
[10] J.C. Vedrine (Ed.), EUROCAT Oxide, Catal. Today 20 (1994).
[11] F. Cavani, C. Cortelli, A. Frattini, B. Panzacchi, V. Ravaglia, F. Trifiro, C. Fumagalli, R. Leanza, G. Mazzoni, Catal. Today 118 (2006) 298.
[12] B. Schimmoeller, H. Schulz, S.E. Pratsinis, A. Bareiss, A. Reitzmann, B. Kraushaar-Czarnetzki, J. Catal. 243 (2006) 82.
[13] D.A. Bulushev, L. Kiwi-Minsker, F. Rainone, A. Renken, J. Catal. 205 (2002) 115.
[14] G.C. Bond, J. Chem. Technol. Biotechnol. 68 (1997) 6.
[15] C.R. Dias, M.F. Portela, G.C. Bond, J. Catal. 157 (1995) 344.
[16] G. Centi, Appl. Catal. A Gen. 147 (1996) 267.
[17] B.M. Weckhuysen, D.E. Keller, Catal. Today 78 (2003) 25.
[18] M. Calatayud, C. Minot, Top. Catal. 41 (2006) 17.
[19] M.G. Nobbenhuis, A. Baiker, P. Barnickel, A. Wokaun, Appl. Catal. A Gen. 85 (1992) 157.
[20] C. Gückel, M. Niedermeier, M. Estenfelder, WO 2005/115616 A1 (2005), to Süd-Chemie AG.
[21] S. Storck, J. Zuehlke, S. Neto, F. Rosowski, WO2004EP05247 20040515 (2004), to BASF AG.
[22] L. Mädler, W.J. Stark, S.E. Pratsinis, J. Mater. Res. 17 (2002) 1356.
[23] I.E. Wachs, S.S. Chan, R.Y. Saleh, J. Catal. 91 (1985) 366.
[24] C. Cristiani, P. Forzatti, G. Busca, J. Catal. 116 (1989) 586.
[25] H.J. Tian, E.I. Ross, I.E. Wachs, J. Phys. Chem. B 110 (2006) 9593.
[26] T. Thoemmes, S. Zuercher, A. Wix, A. Reitzmann, B. Kraushaar-Czarnetzki, Appl. Catal. A Gen. 318 (2007) 160.
[27] R. Strobel, S.E. Pratsinis, J. Mater. Chem. 17 (2007) 4743.
[28] A. Kobata, K. Kusakabe, S. Morooka, AIChE J. 37 (1991) 347.
[29] R.N. Grass, S. Tsantilis, S.E. Pratsinis, AIChE J. 52 (2006) 1318.
[30] R. Strobel, A. Baiker, S.E. Pratsinis, Adv. Powder Technol. 17 (2006) 457.
[31] C. Leroux, G. Nihoul, G. Van Tendeloo, Phys. Rev. B 57 (1998) 5111.
[32] G.T. Went, S.T. Oyama, A.T. Bell, J. Phys. Chem. 94 (1990) 4240.
[33] D.E. Keller, T. Visser, F. Soulimani, D.C. Koningsberger, B.M. Weckhuysen, Vib. Spectrosc. 43 (2007) 140.
[34] N. Magg, B. Immaraporn, J.B. Giorgi, T. Schroeder, M. Baumer, J. Dobler, Z.L. Wu, E. Kondratenko, M. Cherian, M. Baerns, P.C. Stair, J. Sauer, H.J. Freund, J. Catal. 226 (2004) 88.
[35] Z. Wu, P.C. Stair, S. Rugmini, S.D. Jackson, J. Phys. Chem. C 111 (2007) 16460.
[36] G.I. Petrov, V.V. Yakovlev, J. Squier, Appl. Phys. Lett. 81 (2002) 1023.
[37] M.C. Heine, S.E. Pratsinis, Ind. Eng. Chem. Res. 44 (2005) 6222.
[38] G. Oliveri, G. Ramis, G. Busca, V.S. Escribano, J. Mater. Chem. 3 (1993) 1239.
[39] D.A.M. Monti, A. Baiker, J. Catal. 83 (1983) 323.
[40] A.I. Anastasov, Chem. Eng. Sci. 58 (2003) 89.
[41] J.N. Papageorgiou, M.C. Abello, G.F. Froment, Appl. Catal. A Gen. 120 (1994) 17.
[42] G.C. Bond, S.F. Tahir, Appl. Catal. 71 (1991) 1.
[43] R.Y. Saleh, I.E. Wachs, S.S. Chan, C.C. Chersich, J. Catal. 98 (1986) 102.